

DOCUMENT CONTROL SHEET

	ORIGINATOR'S REF. NLR-TP-2003-441	SECURITY CLASS. Unclassified				
ORIGINATOR National Aerospace Laboratory NLR, Amsterdam, The Netherlands						
TITLE Fatigue of air supply manifold support rods in military jet engines						
to the journal "Practical Failure Analysis"						
PERMISSION						
AUTHORS R.J.H. Wanhill	DATE September 2003	<table border="1" style="width: 100%; border-collapse: collapse;"> <tr> <td style="width: 50%;">PP</td> <td style="width: 50%;">REF</td> </tr> <tr> <td style="text-align: center;">23</td> <td style="text-align: center;">13</td> </tr> </table>	PP	REF	23	13
PP	REF					
23	13					
DESCRIPTORS Keywords: fatigue, Inconel 718 rods, jet engine, diffuser air supply						
ABSTRACT <p>Bending fatigue failure occurred in a support rod linking the bleed air supply manifold to the diffuser case in a military jet engine. Other rods were subsequently found cracked. The rods were wrought Inconel 718, operating at about 550 °C. The bending was caused by relative movements of two expansion sleeves held together by the rods, whereby accommodatory swivelling of the spherically-rounded ends of the rods in the mating seatings of the inner sleeves was prevented by contact pressure, fretting and binding. The main reason for binding would have been decomposition of the anti-galling compound applied to the contact surfaces. Fractographic analysis and oxidation interference colours enabled interpreting the cracking history of the broken rod. Elementary stress and fracture mechanics calculations indicated that the maximum fatigue stress would have been below the stress needed to "unlock" the spherically-rounded rod end from its seating.</p>						



NLR-TP-2003-441

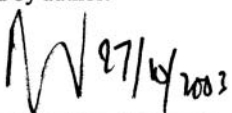
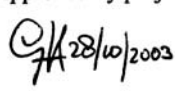
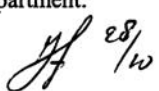
Fatigue of air supply manifold support rods in military jet engines

R.J.H. Wanhill

This report is based on an article submitted to the journal "Practical Failure Analysis".

This report may be cited on condition that full credit is given to NLR and the authors.

Customer: National Aerospace Laboratory NLR
Working Plan number: S.1.B
Owner: National Aerospace Laboratory NLR
Division: Structures and Materials
Distribution: Unlimited
Classification title: Unclassified
September 2003

Approved by author:  27/4/2003	Approved by project manager:  28/10/2003	Approved by project managing department:  28/10
--	--	---



Contents

Introduction	5
Scope of the Failure Analysis	5
Fractography	5
Macrofractography	5
Microfractography	6
Striation and "Beach Marking" Counts	6
Oxidation Interference Colours on Fracture Surfaces	7
Introduction	7
The Broken Rod	7
Furnace Oxidation of Fatigue Fracture Surfaces	7
Comparison of Broken Rod and Furnace Oxidation Interference Colours	8
Other Checks	8
Rod Dimensions, Surface Roughness, Microstructures and Hardness	8
Fretting and Binding	9
Stress Estimates for the Broken Rod	9
Tensile and Bending Stresses from Bleed Air Operation	9
Fatigue Stresses from the Stage I → Stage II Transition	10
Discussion	11
Fracture Surface Details and Engine Operating History	11
Source of Fatigue	13
Conclusions and Recommendations	13
Acknowledgement	14
References	14

2 Tables

10 Figures

(22 pages in total)



Fatigue of air supply manifold support rods in military jet engines

R.J.H. Wanhill*

Abstract

Bending fatigue failure occurred in a support rod linking the bleed air supply manifold to the diffuser case in a military jet engine. Other rods were subsequently found cracked. The rods were wrought Inconel 718, operating at about 550 °C. The bending was caused by relative movements of two expansion sleeves held together by the rods, whereby accommodatory swivelling of the spherically-rounded ends of the rods in the mating seatings of the inner sleeves was prevented by contact pressure, fretting and binding. The main reason for binding would have been decomposition of the anti-galling compound applied to the contact surfaces. Fractographic analysis and oxidation interference colours enabled interpreting the cracking history of the broken rod. Elementary stress and fracture mechanics calculations indicated that the maximum fatigue stress would have been below the stress needed to "unlock" the spherically-rounded rod end from its seating.

Keywords: fatigue, Inconel 718 rods, jet engine, diffuser air supply

* National Aerospace Laboratory NLR, Amsterdam, The Netherlands. Contact e-mail: wanhill@nlr.nl



This page is intentionally left blank.



Introduction

An in-flight fire warning occurred in a military jet aircraft. Post-flight inspection showed that a bleed air supply manifold support rod had broken, see figure 1. This rod had held together two expansion sleeves linking the compressor bleed air supply manifold to the turbine diffuser, see figure 2. Fracture of the rod allowed separation of the expansion sleeves and hot (550 °C) bleed air to impinge on the surrounding airframe.

The rod material was the nickel-base superalloy Inconel 718, conforming to AMS 5663 and given the standard heat treatment of 955 °C/1 hour, air cool, and duplex ageing at 720 °C/8 hours and 620 °C/8 hours.

The engine operating history for the broken rod is given in table 1. Each maintenance, both for this and other rods, would have required loosening and re-tightening the expansion sleeves held together by the rods. Normally this would allow arbitrary rotation of each rod about its longitudinal axis.

Scope of the Failure Analysis

Table 2 shows the scope of the failure analysis. Some noteworthy points are:

- Cracks in radii leading to the spherically-rounded ends of the broken rod and two other rods. These cracks were broken open for fractographic investigation.
- Oxidation interference colours on fatigue fracture surfaces aided interpretation of the service failure.
- Static and fatigue stress estimates were made, needing very different methods.

Fractography

Macrofractography

Figures 3 and 4 show the actual and schematic fracture surfaces of the broken rod. There were two locations of fatigue initiation and crack growth. The older fatigue area shows both 1st and 2nd order interference colours (discussed later) and is centered on the 2 o'clock position in figures 3 and 4. The more recent main fatigue crack shows 1st order interference colours and is centered on the 6 o'clock position. The shapes of the early fatigue crack fronts are diagnostic for



fatigue controlled by bending stresses rather than axial stresses, as is the fact that the older crack stopped growing: this is explained in the discussion section of the paper.

Post-incident nondestructive inspection of ten long-service support rods, including those from the incident engine, revealed cracks in the radii leading to the spherically-rounded ends of the broken rod and two other rods, one of which came from the 4 o'clock diffuser position in the incident engine, see figure 2. These cracks were broken open and proved to be shallow, less than 0.5 mm deep, but up to 4.5 mm long at the surface. This again indicated fatigue controlled by bending stresses. There were three small cracks in the second half of the broken rod, all showing only 2nd order interference colours, such that the cracks might have stopped or were growing very slowly. The other cracks, nine (!) from two rods, showed 1st and 2nd order interference colours, indicating they were still growing, but slowly. Nevertheless, the number of cracks pointed to a potentially widespread problem.

Microfractography

Figure 4 indicates that the main fatigue fracture surface of the broken rod consisted of Stage I and Stage II fatigue. This was inferred from changes in fracture topography, figure 5, and similar topographical changes on less-oxidised fatigue fracture surfaces from a cracked rod and low-cycle fatigue (LCF) specimens from a test programme^[1]. Stage I fatigue is common in precipitation - strengthened nickel-base superalloys, like Inconel 718, and occurs in both LCF and high-cycle fatigue^[2].

Besides a change in fatigue fracture topography, figure 5 shows numerous "beach markings" representing positions of the Stage II fatigue crack front. Figure 6 is a detail of the Stage II fracture surface, showing virtually complete coverage by fatigue striations. This was also the case for the Stage II fracture surfaces of the broken-open cracks.

Striation and "Beach Marking" Counts

The predominance of fatigue striations on the Stage II fracture surface of the main crack in the broken rod prompted striation and "beach marking" counts. Numerous measurements of striation spacings resulted in an estimate of 14,500 cycles for the entire Stage II region, see figure 4. This is LCF.

The "beach markings" were potentially of more interest, since they probably represent peak load excursions during engine operation, and might enable estimating the number of flights during Stage II fatigue crack growth. The Stage II fatigue fracture surface was mapped *completely* at a



magnification of 200X, with details at up to 1000X. The mapping revealed periodic large fatigue striations. These were counted by two independent investigators. Figure 7 shows the results related to the main crack depth and the broad divisions of oxidation interference colours. If the large striations were to correspond to starting the engine, then figure 7 would indicate a Stage II fatigue life of about 250 flights. However, as argued in the discussion section of this paper, it is most likely that the large striations represent peak load excursions that occurred more than once per flight.

Oxidation Interference Colours on Fracture Surfaces

Introduction

The sequence of oxidation interference colours on metallic surfaces is well-known^[3]. For the present investigation their primary significance lay in estimating, however approximately, the elevated temperature exposure times for the main fatigue fracture surface of the broken rod. There are several potential limitations to this use of interference colours. These include any changes in fracture mechanism, fracture surface roughness, cycle frequency and peak load effects. However, except for a change in fracture mechanism, the other influences appear to be minor: the single most important influence on the interference colours is the exposure temperature^[4].

The Broken Rod

The actual and schematic fracture surfaces are shown in figures 3 and 4. The minor fatigue crack at the 2 o'clock position showed 2nd order interference colours down to blue at the circumference of the rod. Under the influence of the main fatigue crack, this older minor crack began to grow again from 2nd order yellow through silver (the silvery hiatus) to the 1st order colours blue, brown and finally yellow.

The main fatigue crack showed predominantly 1st order interference colours, notably in the Stage II fatigue region. An unusual aspect of these colours is the submacroscopic bands within the main zones of colours. These bands undoubtedly portray crack front positions during fatigue crack growth. The question is: what do these crack fronts represent? This is considered in the discussion section of this paper.

Furnace Oxidation of Fatigue Fracture Surfaces

Two Inconel 718 compact tension (CT) specimens with large areas of Stage II fatigue crack growth, obtained at room temperature, were available from a test programme^[1]. The fracture



surfaces were sliced in the crack growth direction and furnace oxidised for different times in air at 550 °C. Figure 8 shows a selection of the results. Within 1 hour the initially metallic grey fracture surfaces became straw yellow. Within 4 hours a mauve/purple colour became dominant. Thereafter, the rate of colour change decreased considerably, as would be expected from the kinetics of oxidation and film thickening^[5], but it was evident that only blue colours were present after about 50 hours oxidation, and that the silvery hiatus was becoming dominant at 370 hours.

Comparison of Broken Rod and Furnace Oxidation Interference Colours

The similarity of the sequence of 1st order interference colours in figures 3 and 8 is evident. The times by which particular colours are obtained from service exposure and furnace oxidation should be similar in magnitude, for the following reasons:

- (1) The service exposure and furnace oxidation temperatures were the same, 550 °C.
- (2) The fatigue fracture topographies were similar, Stage II fatigue striations.
- (3) The likelihood that the overpressure of the bleed air, up to 25 atm (2.5 MPa) in the air supply manifold would have little or no effect on crack tip oxidation kinetics. This assertion is based on the fact that it is the *partial* pressure of oxygen that controls crack tip oxidation in Inconel 718^[6], and not the absolute pressure. (Nevertheless, if the bleed air overpressure were to affect the oxidation kinetics, the effect would be to increase the rate of oxidation and shorten the service times to attain particular colours.)

Figure 8 shows that silver became dominant after furnace oxidation for 370 hours, but figure 3 shows that Stage II fatigue began in the light blue region, with some Stage I fatigue also in the light blue region. Thus Stage II fatigue in the broken rod probably took considerably less than 370 hours. This is returned to in the discussion section of this paper.

Other Checks

Rod Dimensions, Surface Roughness, Microstructures and Hardness

The same ten long-service rods, including those from the incident engine, were checked for dimensions, surface roughness, microstructures and hardness. There were no evident anomalies that might help to explain why cracks occurred in the broken rod and two other rods. However, the blending radii between changes in rod cross-section sometimes had small irregularities^[7].



Fretting and Binding

All ten long-service rods showed local fretting on the spherically-rounded ends. The Technical Order (T.O.) specified installing the support rods with an anti-galling compound (MoS₂ + binder) on the expansion sleeve mating seatings. The spherically-rounded end of the broken rod was examined by Energy Dispersive analysis of X-rays (EDX), and a molybdenum peak was found, indicating that MoS₂ had been used during expansion sleeve/support rod installation.

However, a NAVAIR T.O.^[8] states that MoS₂ is not stable above 427 °C and should not be used at higher temperatures. Also, MoS₂ rapidly loses its lubricating ability in high pressure air above 300 °C^[9]. Thus it is likely that some, if not all, air supply manifold support rods experienced fretting and also binding, such that they could not provide accommodatory swivelling of the spherically-rounded ends in the mating seatings of the expansion sleeves. In fact, inspection of five engines revealed that one rod was immovable without considerable force: it should have moved freely when the inner and outer expansion sleeves were disconnected. Note that the accommodatory swivelling does *not* involve rotation of the rod about its longitudinal axis: this cannot occur except during disassembly and reassembly.

Stress Estimates for the Broken Rod

Tensile and Bending Stresses from Bleed Air Operation

1. *Uniform tensile stress in rod.* When the engine starts, the air supply manifold pressurizes to a maximum of 25 atm (2.5 MPa). The support rod is then under tensile stress, given by $P(D_1/D_2)^2$, where P is the pressure, D₁ is the internal diameter of the expansion sleeve cap, and D₂ is the rod diameter. Assuming P = 2.5 MPa, D₁ = 68 mm, and D₂ = 8 mm (see figure 1), the maximum uniform tensile stress in the rod is $\sigma_{ut,max} = 183$ MPa.
2. *Contact stress from pressure on the spherically-rounded end.* Figure 9 is a diagram of the situation, with definitions of force and contact stress. Assuming D₂ = 8 mm, $\sigma_{ut} = 183$ MPa, $\alpha = 27^\circ$, average R₃ = 10.25 mm, and h ~1 mm, the maximum contact stress is $\sigma_{c,max} = 315$ MPa. This contact stress is substantial and could prevent swivelling, depending on the friction between the rod end and the mating seating of the expansion sleeve.
3. *Swivelling moment on the spherically-rounded end.* Since the spherically-rounded end experiences a substantial contact stress, a moment is required to swivel it. The swivelling moment M towards the rod axis is defined in figure 9. Assuming the above values of D₂, σ_{ut} , α and R₃, and a low value of the coefficient of friction, $\eta = 0.2$, then M = 23.56 N.m.

4. *Tensile + bending stress in rod.* The maximum tensile stress in the main cylindrical part of the rod is in the outermost fibre and is due to uniform tension + bending stresses. Specifically, $\sigma_{t,max} = \sigma_{ut,max} + M(D_2/2) / I$, where I is the second moment of area, equal to $\pi(D_2)^4 / 64$. Assuming the above values of D_2 , $\sigma_{ut,max}$ and M , then $\sigma_{t,max} = 652$ MPa.

These calculations show that even a fairly low value of the coefficient of friction, $\eta = 0.2$, could require a maximum tensile stress of about 650 MPa to be reached at the surface of the main cylindrical part of the rod before it would swivel to accommodate any relative movements of the inner and outer expansion sleeves during engine operation. In unfavourable circumstances (binding) the value of η , and hence $\sigma_{t,max}$, could be much higher.

Furthermore, these calculations indicate a dominating contribution of bending stress. The shapes of the early fatigue crack fronts in the broken and cracked rods, for example figure 3, are consistent with stresses primarily due to bending.

Fatigue Stresses from the Stage I → Stage II Transition

At a crack depth of 0.54 mm the main crack in the broken rod made a transition from Stage I to Stage II fatigue, see figure 5. According to Runkle and Pelloux^[2] such transitions depend on the crack tip cyclic plastic zone size becoming larger than the grain size. Under nominally plane strain conditions the cyclic plastic zone has a "butterfly-wing" shape, with its longest dimension, r_y^c , roughly normal to the path of the fatigue crack. From Wanhill and Looije^[10]:

$$r_y^c = 0.05 \left(\Delta K_{eff} / \sigma_y^c \right)^2 \quad (1)$$

where ΔK_{eff} is the effective stress intensity factor range in fatigue, and σ_y^c is the cyclic yield stress. Assuming r_y^c corresponds to the average grain size (6.5 μm for the broken rod) at the transition from Stage I to Stage II fatigue, and that $\sigma_y^c = 769$ MPa at 550 °C (derived from Heuler and Bergmann^[11]), then substitution into eq. (1) gives $\Delta K_{eff} = 8.77$ MPa $\sqrt{\text{m}}$.

During engine operation the largest cycles (start-stop) will have a stress ratio $R=0$. For this R value a plane strain calculation^[11] gives $\Delta K_{eff} = 0.75 \Delta K = 0.75 K_{max}$. Assuming that the largest regularly-occurring cyclic plastic zone determines the transition from Stage I to Stage II fatigue, see Wanhill and Looije^[10], then the maximum stress intensity factor at the transition is $K_{max} = \Delta K_{eff} / 0.75$. Substituting $\Delta K_{eff} = 8.77$ MPa $\sqrt{\text{m}}$ gives $K_{max} = 11.7$ MPa $\sqrt{\text{m}}$.



Now consider the main crack shown in figures 3 and 4. At the transition from Stage I to Stage II fatigue the crack shape is approximated by a partly annular surface flaw with a depth-to-length ratio of 0.06. For this geometry, with a crack depth of 0.54 mm in an 8 mm diameter rod, the NASA/FLAGRO SC09 stress intensity factor solution for a crack in bending^[12] gives $K/\sigma = 0.048 \sqrt{m}$. Substituting $K_{\max} = 11.7 \text{ MPa} \sqrt{m}$, and writing σ_{\max} for σ , gives $\sigma_{\max} = 244 \text{ MPa}$.

The maximum fatigue stress at the rod surface would have been higher, for two reasons. First, the tensile bending stress would be higher, but no more than about 260 MPa even if the rod were in pure bending, rather than a likely combination of tension and bending. Second, the fatigue crack occurred at a stress concentration owing to the change in cross-section and blending radius, see figure 1. From Peterson^[13] the appropriate stress concentration factor is $K_t = 1.43$. The local maximum fatigue stress would then be more than 370 MPa.

On the one hand, this value of local maximum fatigue stress is much less than the local maximum tensile stress ($652 \times 1.43 = 932 \text{ MPa}$) required before the rod could swivel. But on the other hand, this local maximum fatigue stress is too low to cause fatigue failure in Inconel 718, even at temperatures higher than $550 \text{ }^\circ\text{C}$ ^[1]. The conclusion must be that the above calculations underestimate the local maximum fatigue stress at the rod surface. One possible cause for this discrepancy is the previously mentioned irregularities in the blending radii, leading to higher stress concentrations.

Be that as it may, the estimates of tensile, bending and fatigue stresses in this section of the paper indicate that fatigue stresses causing crack initiation and growth occurred in the broken rod because it was unable to swivel to accommodate relative movements of the inner and outer expansion sleeves of the bleed air assembly.

Discussion

Fracture Surface Details and Engine Operating History

The fractography showed that fatigue cracking of the rods was controlled by bending stresses. An estimate of 14,500 cycles was obtained for the Stage II fatigue fracture of the main crack in the broken rod from the incident engine. The number of large fatigue striations in this fracture region was about 250.



From the oxidation interference colours it was concluded that the secondary fatigue crack on the fracture surface of the broken rod was older than the main crack. The main crack showed 1st order interference colours in Stage II fatigue. Furnace oxidation tests indicated that this Stage II fatigue occurred well within 370 hours of service operation. However, an exclusive feature of the service failure was the presence of submacroscopic interference colour bands on the Stage II fatigue fracture surface.

Figure 10 is a summary linking the broken rod fracture surface details with the engine operating history. The secondary crack ① was the first to occur, by bending fatigue. As a result of the first maintenance, the rod was re-installed with an axial rotation such that further growth of the secondary crack was inhibited. Bending fatigue then initiated the main crack by Stage I fatigue ② .

The table in figure 10 gives the most probable history of formation of the main crack fatigue fracture surface. An essential point is that the 2nd maintenance resulted in the rod being in a similar orientation to that between the 1st and 2nd maintenances. Although this might seem unlikely, the alternative would be that the entire main crack grew to failure during the short period between 2nd maintenance and failure. This is incompatible with the interference colour evidence, since a fully completed silvery hiatus would require several hundred hours, see figure 8.

The most probable history of the main fatigue crack is that most – or all – of the fatigue fracture area ② formed during the period between 1st and 2nd maintenance. This leaves the period from 2nd maintenance to failure, 143.5 engine operating hours, as the maximum amount of time to form the fatigue fracture areas ③ and ④. This rationale is compatible with the interference colours on the fracture surface. Furthermore, there were about 55-60 of the submacroscopic interference colour bands on areas ③ and ④. This number agrees well with the number of flights, 57, from 2nd maintenance to failure, and is likely to be no coincidence. Instead, these submacroscopic bands could represent oxidation effects from flight-by-flight heating and cooling, which was not possible in the furnace oxidation tests.

Summarising, it appears most probable that Stage II fatigue crack growth took place between 2nd maintenance and failure, i.e. within 143.5 engine operating hours. This means that the number of large striations in Stage II fatigue, estimated to be about 250, corresponds to a maximum of 57 flights. Consequently, the large striations represent peak load excursions that occur more than once per flight. This is reasonable for military jet engines.



Source of Fatigue

From the fractographic evidence (crack front shapes), the fretting and binding of the spherically-rounded ends of the rods, the temperature capability of MoS₂ as a lubricant, and the self-consistency of the estimated tensile, bending and fatigue stresses, it is reasonable to conclude that bending stresses were responsible for fatigue cracking, and that these bending stresses were due to the rods being unable to swivel to accommodate relative movements of the inner and outer expansion sleeves of the bleed air assembly. In turn, the accommodatory swivelling was prevented because the MoS₂ anti-galling compound would have decomposed and lost its function at temperatures below the normal operating temperature of the bleed air assembly.

Conclusions and Recommendations

Investigation of several air supply manifold support rods, including one broken and two cracked, led to the following conclusions:

- (1) The fractures in the broken and cracked rods resulted from bending fatigue. The bending was caused by relative movements of two expansion sleeves held together by the rods, whereby accommodatory swivelling of the spherically-rounded ends of the rods in the mating seatings of the inner sleeves was prevented by contact pressure, fretting and binding. The main reason for binding would have been decomposition of the anti-galling compound applied to the contact surfaces. This compound consisted of MoS₂ and a binder, and would have lost its lubricating ability well below the operating temperature of the bleed air assembly.
- (2) The main fatigue crack in the broken rod showed a transition from Stage I to Stage II fatigue. The remaining fatigue life in Stage II was no more than 57 flights, corresponding to 143.5 hours of engine operation. This assertion is based on the oxidation interference colours present on the fatigue fracture surface and on submacroscopic colour bands within the main zones of colours.

This investigation led to two obvious recommendations. First, all the other air supply manifold support rods in service should be inspected for cracks. This would be a regular addition to the normal maintenance T.O. Second, the MoS₂ + binder anti-galling compound should be replaced by a compound with temperature capability well above 600 °C. Both recommendations were implemented.



Acknowledgement

The tensile and bending stress estimates were made by H.H. Ottens of the NLR.

References

1. P. Heuler and J.W. Bergmann, "IEPG TA 31, a Research Programme into Lifting Concepts for Military Aero-Engine Components", Final Report B-TA-3602, Industrieanlagen-Betriebsgesellschaft mbH (IABG), Ottobrunn, Germany, August 1997.
2. J.C. Runkle and R.M. Pelloux, "Micromechanisms of low-cycle fatigue in nickel-based superalloys at elevated temperatures", *Fatigue Mechanisms*, ASTM Special Technical Publication 675, J.T. Fong, Ed., ASTM, Philadelphia, PA 19103, 1979, pp. 501-524.
3. U.R. Evans, *The Corrosion and Oxidation of Metals, Second Supplementary Volume*, Edward Arnold, London, UK, 1976, p. 379.
4. T.C. Radtke, Personal Communication from the Aeronautical and Maritime Research Laboratory (AMRL), Melbourne, Australia, 23 March 1993.
5. U.R. Evans, *The Corrosion and Oxidation of Metals: Scientific Principles and Practical Applications*, Edward Arnold, London, UK, 1971, pp. 27-28.
6. E. Andrieu, H. Ghonem and A. Pineau, "Two-stage crack tip oxidation mechanism in alloy 718", *Elevated Temperature Crack Growth*, MD-Vol. 18, S. Mall and T. Nicholas, Eds., The American Society of Mechanical Engineers, New York, N.Y. 10017, 1990, pp. 25-29.
7. R.J.H. Wanhill, J.A.M. Boogers, H.N. Huisman and H.H. Ottens, "Failure and Cracking of Inconel 718 Air Supply Manifold Support Rods", NLR TP 96047 L, National Aerospace Laboratory NLR, Amsterdam, The Netherlands, January 1996.
8. Department of the Navy, NAVAIR Technical Order 02-1-517/T.O. 2-1-111/DMWR 55-2800-206, February 1990, p. 21-2.
9. H.E. Sliney, "Solid Lubricants", *ASM Handbook Volume 18, Friction, Lubrication, and Wear Technology*, P.J. Blau, Ed., ASM International, Materials Park, OH 44073, 1992, pp. 114-115.



10. R.J.H. Wanhill and C.E.W. Looije, "Fractographic and Microstructural Analysis of Fatigue Crack Growth in Ti-6Al-4V Fan Disc Forgings", AGARD Report 766 (Addendum), Advisory Group for Aerospace Research and Development, Neuilly-sur-Seine, France, April 1993, pp. 2.1 – 2.40.
11. J.C. Newman, Jr., "A Crack-Closure Model for Predicting Fatigue Crack Growth Under Aircraft Spectrum Loading", *Methods and Models for Predicting Fatigue Crack Growth Under Random Loading*, J.B. Chang and C.M. Hudson, Eds., ASTM STP 748, ASTM, Philadelphia, PA, 1981, pp. 53-84.
12. Fatigue Crack Growth Computer Program NASA/FLAGRO Version 2.0, Annex 2 in ESACRACK User's Manual, ESA PSS-03-209 Issue 2, European Space Agency, Paris, France, 1995.
13. R.E. Peterson, *Stress Concentration Design Factors*, John Wiley & Sons, Inc., New York, 1953, p. 74.



Table 1 Broken rod engine operating history

Service History	Intervals		
	Operating Hours	LCF cycles	Flights
0 → 1st maintenance	410.9	2361	257
1st → 2nd maintenance	761.5	3082	326
2nd maintenance → failure	143.5	343	57
Total	1315.9	5786	640

Table 2 Scope of the failure analysis

Fractography: broken rod and forcibly opened cracks in broken and unbroken rods
Crack shapes, fatigue origins, Stage I and Stage II fatigue crack growth, striation counts
Oxidation interference colours on fracture surfaces
Broken and cracked rods, compact tension fatigue test specimens
Other checks
Rod dimensions and surface roughness
Microstructures and hardness
Fretting and binding of spherically-rounded rod ends
Stress estimates for the broken rod
Tensile and bending stresses: derivation from operating conditions
Fatigue stresses: derivation from Stage I → Stage II fatigue transition

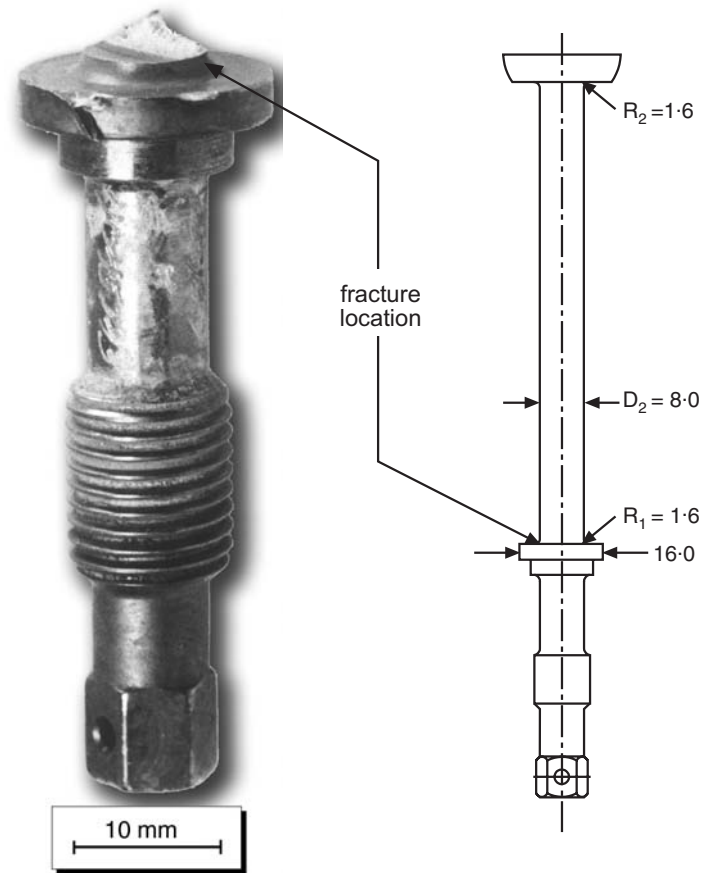


Fig. 1 Broken rod, and sketch of intact rod, showing spherically-rounded end. Indicated dimensions are nominal (mm)

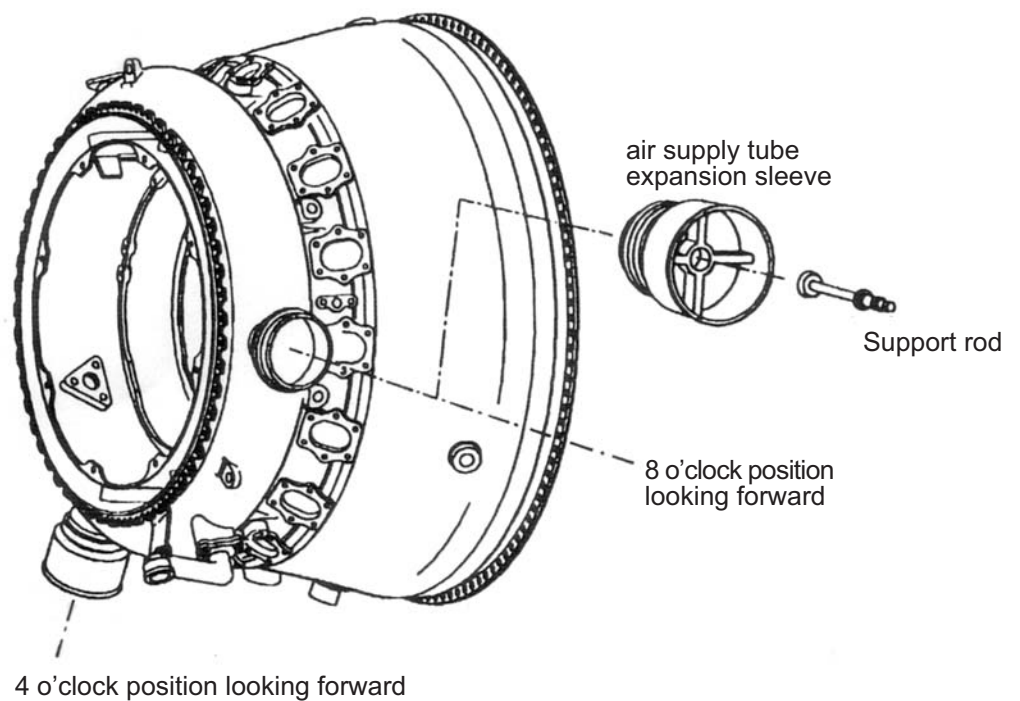


Fig. 2 Diffuser case and one air supply tube expansion sleeve and a support rod (broken in the incident engine)

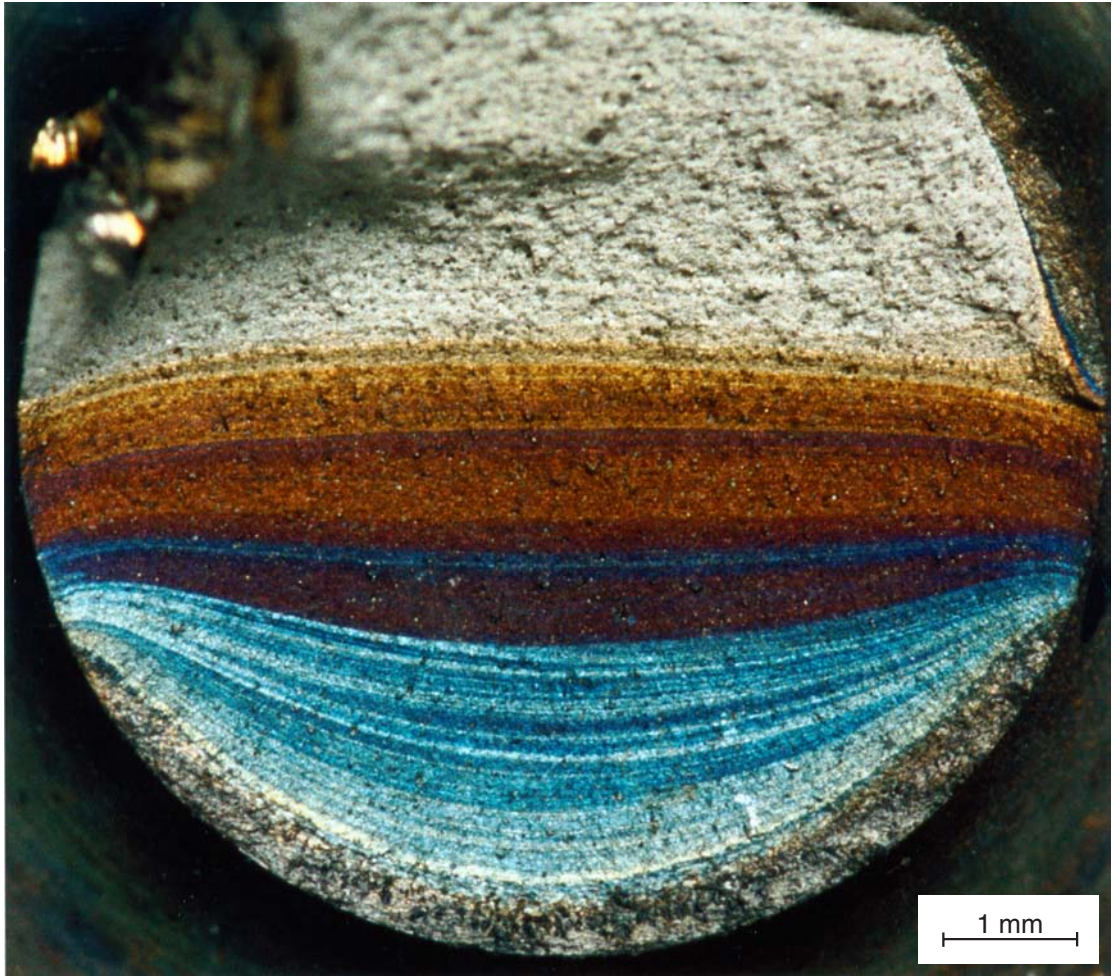


Fig. 3 Macro photograph of the fracture surface of the broken rod

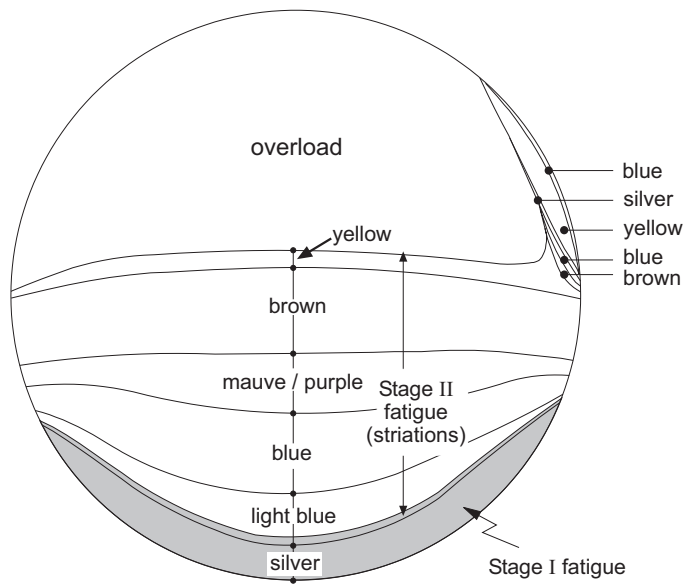


Fig. 4 Schematic of the fracture surface of the broken rod, listing fracture characteristics and oxidation interference colours

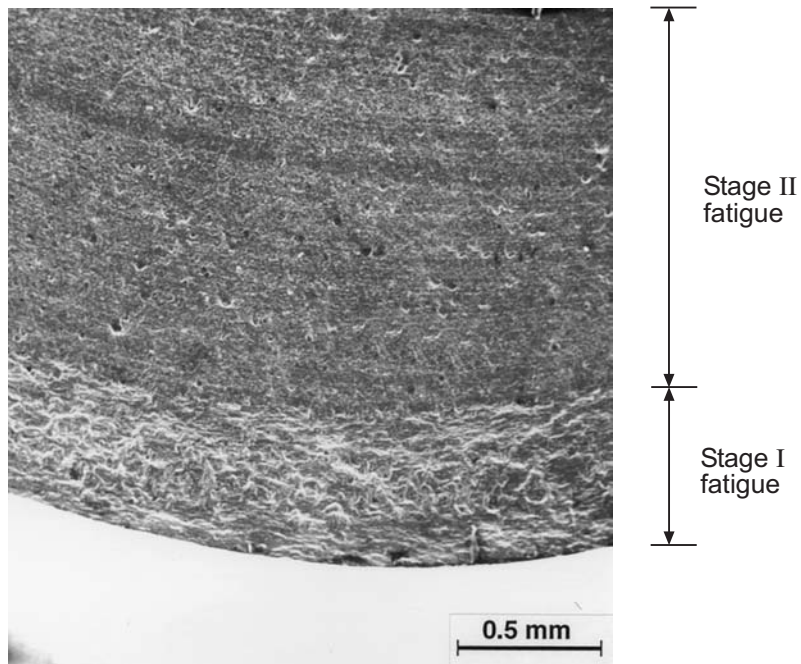


Fig. 5 SEM mesofractograph of Stage I → Stage II fatigue transition for the main crack in the broken rod: see figure 4 also

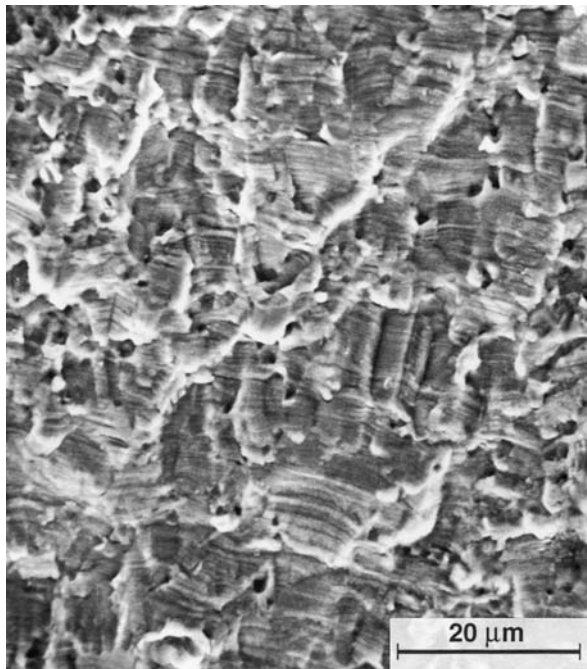


Fig. 6 Detail of figure 5 in the Stage II region, showing fatigue striations

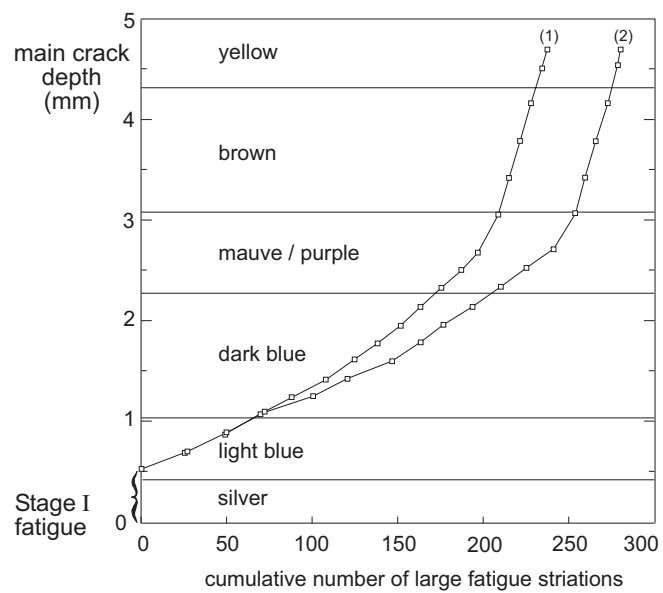
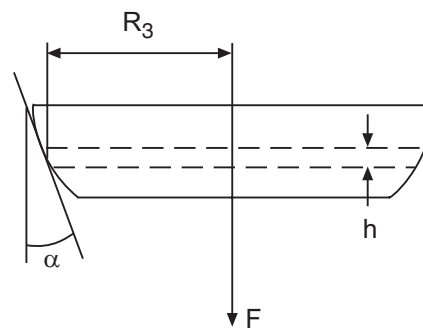


Fig. 7 Cumulative number of large striations for the Stage II fatigue region of the main crack in the broken rod: (1) and (2) are independent measurements by two fractographers



Fig. 8 Furnace oxidation of Inconel 718 Stage II fatigue fracture surfaces at 550 °C

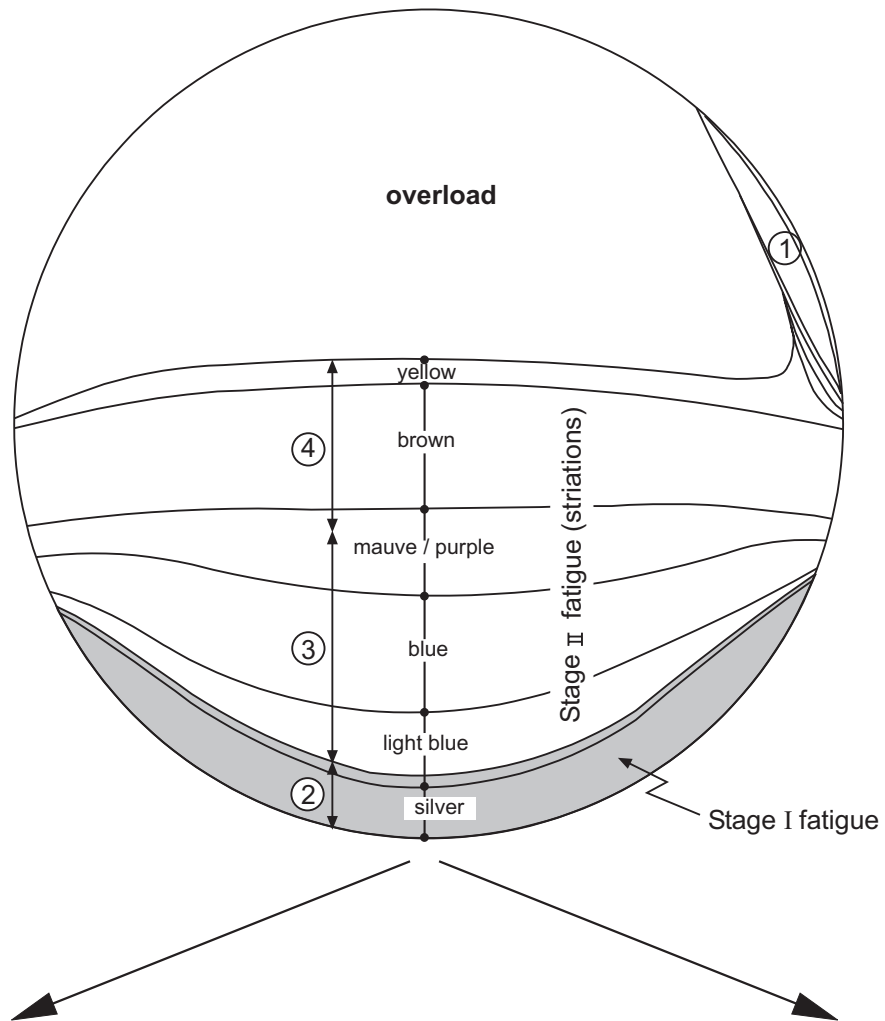


$$\text{Force } F = \frac{\pi}{4} (D_2)^2 \cdot \sigma_{ut}$$

$$\text{Contact stress } \sigma_c = F / (\sin \alpha \cdot 2\pi R_3 h)$$

$$\text{Swivelling moment } M = 2\eta F R_3 / (\pi \tan \alpha)$$

Fig. 9 Force, contact stress and swivelling moment for a spherically-rounded rod end; η is the coefficient of friction; D_2 is the rod diameter, see figure 1. See text for quantification of the formulae



Service History	Intervals			Fatigue fracture areas
	Operating hours	LCF cycles	Flights	
0 → 1st maintenance <i>rod rotation</i>	410.9	2361	257	①
1st → 2nd maintenance <i>no rod rotation?</i>	761.5	3082	326	②
2nd maintenance → failure	143.5	343	57	③ + ④

Fig. 10 Interpretation of the relation between fatigue fracture areas and engine operating history for the broken rod